Role of Phase Behavior and Atomization in the Supercritical Antisolvent Precipitation

ARTICLE *in* INDUSTRIAL & ENGINEERING CHEMISTRY RESEARCH · SEPTEMBER 2003

Impact Factor: 2.59 · DOI: 10.1021/ie0302138

3 AUTHORS, INCLUDING:

E. Reverchon
Università degli Studi di Salerno
255 PUBLICATIONS **8,012** CITATIONS
SEE PROFILE

Iolanda de marco
Università degli Studi di Salerno
52 PUBLICATIONS **1,528** CITATIONS
SEE PROFILE

Role of Phase Behavior and Atomization in the Supercritical Antisolvent Precipitation

Ernesto Reverchon,* Giuseppe Caputo, and Iolanda De Marco

Dipartimento di Ingegneria Chimica e Alimentare, Università degli Studi di Salerno, Via Ponte Don Melillo, 84084 Fisciano (SA), Italy

An experimental study on supercritical antisolvent (SAS) precipitation has been performed to gain insight into the role of phase behavior and atomization in controlling morphology and dimension of precipitates. The mixture yttrium acetate/dimethyl sulfoxide has been used as the main model system and supercritical CO_2 has been used as the antisolvent. Two SAS apparatuses (laboratory and pilot scale) with two injector arrangements and operating with various injector diameters in the range 60−500 μm have been used. The results showed that operating above the mixture critical point (MCP) of the ternary mixture yttrium acetate/dimethyl sulfoxide/carbon dioxide, sub-micrometric particles are generated nearly independently from the size of the injector and of the apparatus. We also demonstrated that it is possible to modify the particle dimension by simply changing the operating pressure and/or temperature in the vicinity of the MCP. The use of a pseudo-binary diagram pressure-molar fraction has been proposed as a base framework to explain the relationship between the particle morphology and the phase behavior of processed mixtures. Particularly, we have shown that the single-phase region in the gas-rich side of the pressure−composition diagram and below the MCP can be usefully explored to modify the particle dimensions of the precipitate.

Introduction

Supercritical antisolvent precipitation is a semicontinuous precipitation technique developed to produce micrometric and sub-micrometric particles that are not attainable by conventional methods. In this process a supercritical fluid (SCF) and a liquid solution are continuously delivered to a high-pressure precipitator in which the SCF forms a solution with the liquid, inducing the precipitation of the dissolved solid. The supersaturation of the solid is rapidly reached by the volumetric expansion of the liquid solution with a time scale of approximately 10^{-5} s[1]. The most attractive characteristics of SAS precipitation are the ability to control particle size and morphology and to eliminate the solvent residue without postprocessing of the produced powders. From a thermodynamics point of view, the SAS process must satisfy the following requirements: the solute must be soluble in the organic solvent at the process temperature and must be insoluble in the SCF. The solvent must be completely miscible with the SCF; otherwise, two fluid phases will be formed and the solute can remain dissolved or partly dissolved in the liquid-rich phase.

Scientific literature contains information on several materials that have been processed by SAS using different apparatuses and conditions. For example, pharmaceuticals, superconductors, catalyst precursors, pigments, and polymers have been prepared using SAS precipitation.[2,3] The results are quite different depending on the process mode and, of course, on the nature of the material and on the fluid phase equilibria characterizing the ternary system. As a general consideration, the mean particle size that can be obtained by SAS precipitation ranges from 0.1 μm to several micrometers. For what concerns the particle shape, spherical amorphous microparticles can be obtained and in several cases crystals have also been produced.

To date, despite the fact that many works have been published on the generation of particles by SAS, only a limited number of papers have focused on the mechanisms controlling particle formation. Indeed, these mechanisms are quite complex because the precipitation is the result of the interplay of fluid dynamics (jet breakup), mass transfer, nucleation kinetics, and thermodynamics (high-pressure ternary phase equilibria). Moreover, particle morphology can be affected by many process parameters such as temperature, pressure, solution concentration, and solution to antisolvent flow rate ratio. The process arrangement and the apparatus can also heavily influence the product properties. The major drawback of this gap of knowledge is a limited development of the SAS process on a large scale. However, many questions concerning the fundamental phenomenology of the process are under discussion, and partial models are available. For example, the role of mass transfer in the particle formation mechanism has been studied by Werling and Debenedetti.[4,5] They considered the diffusion between a single stagnant droplet of toluene of fixed initial radius and the SC−CO_2 phase and established the time-dependent behavior of such droplet. The numerical solution of conservation equations and of an equation of state allowed them to describe the droplet composition, the density, and the radius change with time. According to this model, the droplet radius varies with time as a function of the rate change in the droplet density and the net molar flux at the interface. The model has been developed for both subcritical and supercritical conditions for a CO_2/toluene mixture. A model that incorporates the effect of jet hydrodynamics, mass transfer, and phase equilibria has been developed by Kikic et al.[6] This model predicts the

* To whom correspondence should be addressed. Fax: 0039 089964057. E-mail:ereverchon@unisa.it.

10.1021/ie0302138 CCC: $25.00
Published on Web 09/06/2003

composition of the phases, the droplet diameter, and the amount of the precipitated product as a function of the liquid velocity, of the injector diameter, and of the gas-to-liquid flow rate. Unfortunately, both these models have not been supported with experimental data.

As a rule, SAS micronization is carried out without a knowledge of the high-pressure phase behavior of the ternary system solvent/antisolvent/solute and of the conditions at which the ternary mixture is supercritical. Therefore, it is difficult to correlate experimental results to phase behavior. A contribution in this direction has been given by Dixon et al.,[7] who presented on a hyphothetical triangular phase diagram the pathways of transformation of a polymer particle as a function of the system composition and predicted the particle morphology on the basis of the position of the operating line with respect to the binodal and spinodal equilibrium curves.

Following a similar approach, the change of particle morphology of acetaminophen precipitated from ethanol with respect to the position of the operating point on the phase diagram of the binary mixture ethanol/CO_2 has been reported.[8] Particularly, it was observed that below the critical point of the binary system, a liquid-rich phase is formed from which large crystals are generated due to supersaturation, and that above the mixture critical point one phase is formed at a high level of supersaturation from which relatively small particles are formed.

Recently, our research group studied the precipitation of Rifampicin from dimethyl sulfoxide (DMSO) using a windowed precipitator, operating at different conditions of pressure and Rifampicin concentration.[9] Nanoparticles with an average dimension of about 400 nm were obtained at conditions where complete miscibility of the ternary mixture Rifampicin/DMSO/CO_2 occurs, whereas microparticles having a mean dimension up to 5 μm were obtained operating at conditions where two fluid phases are formed. An explanation of the different morphologies observed was attempted, considering that a modification of the high-pressure vapor−liquid equilibria toward higher critical pressures occurred in the ternary system DMSO/CO_2/Rifampicin with respect to the behavior of the binary system DMSO/CO_2.

The role of liquid jet breakup on the particle formation mechanism has been studied by different authors[10,11] and also various injection devices have been proposed in the literature.[3] However, the influence of fluid dynamics on particle morphology is not yet well-understood. An effort in this direction has been proposed by Lengsfeld et al.,[12] who studied the change of surface tension in fluid injected into compressed CO_2 to determine the mechanism of atomization. They demonstrated that since, at supercritical conditions surface tension of the liquid approaches zero at a distance shorter than characteristic breakup length, distinct droplets are not formed. These authors proposed that microparticle formation results from gas-phase nucleation and growth within the expanding plume rather than by nucleation within discrete liquid droplets. The results of Lengsfeld et al.[12] basically explain the micronization mechanism in the case of miscible systems above the mixture critical pressure. Moreover, reviewing literature data, they observed that the effect of fluid velocity and injection geometry on particle dimension is of minor importance. A similar conclusion was also reached by other authors.[13,14]

Therefore, from the analysis of the works until now published, a lack of information exists in the correlation between the particle morphology and the main phenomena governing the process: particularly jet breakup, mass transfer, and phase equilibria.

The aim of this work is to produce data targeted to the understanding of the role of jet breakup and phase equilibria in controlling the morphology of precipitates. Two SAS apparatuses (laboratory and pilot scale) with two injector arrangements and operating with various injector diameters have been used. The experiments are performed at selected values of pressure and temperature using the mixture yttrium acetate/DMSO, which has been chosen as a model system since its processability by SAS was previously successfully demonstrated.[15] As a comparison, also experimental data obtained using other solvent/solute couples are used in the Discussion section.

Experimental Section

Materials and Methods. Yttrium acetate (YAc), purity 99.9%, and dimethyl sulfoxide (DMSO), purity 99%, were bought from Aldrich. Untreated YAc crystals ranged from about 20 to 200 μm. We measured a solubility of YAc in DMSO of about 320 mg/mL at 20 °C. The powder collected in the precipitator was observed by a scanning electron microscope (SEM) (model LEO 420). Samples were covered with 250 Å of gold using a sputter coater (Agar model 108A). Particle size of each sample was evaluated by measuring about 600−800 particles from different images using image analysis software (SigmaScan Pro 5). Particle size distributions (PSD) were obtained and the mean particle size was calculated as the number-average diameter.

Apparatuses and Procedures. Bench-Scale Apparatus. The configuration of this SAS apparatus consists of an HPLC pump equipped with a pulse dampener used to feed the liquid solution and a diaphragm high-pressure pump used to deliver carbon dioxide. A cylindrical vessel of 0.5 dm^3 (i.d. 5 cm) was used as the precipitation chamber. The liquid mixture was sprayed in the precipitator through a thin wall stainless steel nozzle. We used a nozzle diameter of 60, 100, and 200 μm. SC−CO_2 was pumped through another inlet port located on the top of the chamber. CO_2 was heated to the process temperature before entering the precipitator. A stainless steel frit was put at the bottom of the chamber to collect the solid product, allowing the CO_2−organic solvent solution to pass through. A more detailed description of this apparatus and procedure can be found in a previous paper.[16]

Pilot-Scale Plant. The pilot plant used in this study is a closed-loop plant consisting mainly of a CO_2 storage vessel, a precipitator, a liquid separator, two pumps, a heat exchanger, and a condenser. The water-jacketed precipitator has an internal volume of 5.2 dm^3 and a L/D ratio of 9.4. The liquid solution and SC−CO_2 are fed to the chamber through a tube-in-tube injection system. The generation of small liquid droplets is ensured by the presence of a 500-μm nozzle fitted on the tip of the internal tube. The injector has been designed to produce a fast contact between the two streams at the outlet of the tubes, where a turbulent flow is generated. Similar coaxial injectors have been used for general purpose atomization[17] and by some authors for SAS processing.[18] A more detailed description of the pilot plant and its representation can be

found in a previous work.[19] The experimental procedure has been described in previous works[16,19] and is similar for both bench- and pilot-scale plants.

Phase Behavior Investigation Apparatus. A constant volume windowed precipitator was used to study the phase behavior of the mixture CO_2/DMSO/YAc during SAS precipitation. The vessel is a stainless steel cylinder of 0.375 dm^3 with two quartz windows put along the longitudinal section of the chamber. A detailed description of the vessel and of the apparatus can be found elsewhere.[9] Experiments were performed following the same procedures adopted for the bench-scale tests. Direct observation through large windows allowed us to follow the macroscopic evolution of the process from the liquid jet breakup to the deposition of precipitated particles.

Experimental Results

Phase Behavior Analysis. Some preliminary experiments were performed to observe the high-pressure phase behavior of the mixture DMSO/CO_2 and to obtain visual information on the liquid jet formation and its evolution. A similar approach has been proposed by other authors in the case of methylene chloride/CO_2[10] and of ethanol/CO_2 mixtures.[11]

The windowed vessel was pressurized with CO_2, and when the desired pressure was reached, CO_2 and DMSO were fed at a constant molar fraction of 0.98 in all the experiments. When we operated at 40 °C, the liquid jet entered deeply in the fluid phase at pressures below 9.0 MPa. At this condition a liquid phase accumulated at the bottom of the precipitator and a meniscus separated it from the upper fluid phase. At pressure slightly higher than 9.0 MPa, the meniscus disappeared and the vessel content showed an orange color, indicative of Rayleigh scattering occurring at the critical transition. When the pressure was increased, a stable and translucent phase filled the vessel and the liquid jet was visible only close to the injector. A further increase of the pressure to 15 MPa produced the almost complete disappearance of the jet. Operating at 50 °C, the formation of the single fluid phase was observed at about 12 MPa, while at lower pressure liquid droplets traveled along the precipitator, on the bottom of which a liquid phase was formed. Finally, operating at 60 °C the single fluid phase was visible starting from 14 MPa, and at 16 MPa the almost complete disappearance of the jet occurred. These observations give indication on the phase behavior for the system DMSO/CO_2 and show that the higher the temperature, the higher the pressure at which the miscibility between DMSO and SC−CO_2 occurs, in accordance with the general behavior of systems of type I in the classification of Konynemburg and Scott[20] that are characterized by the complete miscibility in the liquid phase. This occurrence is characteristic of systems formed by a supercritical component and a medium volatility compound. The large compilation of high-pressure vapor−liquid equilibria presented by Ohe[21] demonstrates that this behavior is characteristic of CO_2 with many organic solvents used in SAS processing. Kordikowski et al.[22] showed that this is also the case of the mixture CO_2/DMSO at 30 °C. Moreover, the visual observation evidenced that the dissolution of the liquid into the supercritical phase is very fast and that, at a fixed temperature, the higher the pressure, the faster the kinetics of liquid dissolution in the SCF.

At this point, we studied the behavior of the ternary system YAc/DMSO/CO_2, operating at 40 °C. Injecting a 1.36 wt % solution of YAc in DMSO at 9.0 MPa (i.e., at miscibility conditions for the binary system) a snowlike powder near the injection system was observed. The powder progressively dispersed in the precipitator and accumulated prevalently on the bottom of the vessel. When the pressure was increased, no phenomenological variations were detected. A similar phenomenon was observed when a 4.5 wt % solution was injected, but in this case the formation of the single phase started at a pressure of 12 MPa, that is, at about 3.0 MPa higher than in the previous case. At pressures lower than 12 MPa the liquid droplets traveled across the whole precipitation chamber and deposited at the bottom of the vessel where a liquid phase formed. When the pressure was increased up to 15 MPa, the precipitation proceeded similarly to that at 12 MPa, but the formation of the solid was faster. In conclusion, no differences in the phase behavior between DMSO/CO_2 and YAc/DMSO/CO_2 systems was observed at the lower concentration of YAc, while at the higher concentration we observed an increase of the pressure at which the transition from a biphasic to a monophasic system occurred. However, this phase behavior of a ternary system at high pressure cannot be generalized and in other cases very different behaviors have been observed.

Effect of the Injector on Particle Morphology. The role of injector type and dimension on the particle morphology of YAc powders has been analyzed by performing a series of experiments on the bench-scale apparatus and on the pilot-scale plant, operating at 15 MPa, 40 °C, 0.98 CO_2 mole fraction, and 4.5 wt % of YAc in DMSO; that is, conditions at which the binary system is completely miscible. The bench-scale apparatus was equipped with thin-wall nozzles of various diameters, from 60 to 200 μm while the pilot plant was equipped with the modified coaxial injector 500 μm in diameter. As previously described, flow arrangement also differs: in the bench-scale operation, liquid solution and SC−CO_2 are fed through two distinct inlet ports, whereas in the pilot-scale operation a tube-in-tube injection is used.

Examples of YAc particles produced in these experiments are shown in Figure 1 where SEM images obtained at the same magnification are presented. These images show that sub-micrometric particles are produced both with the small and the larger injector. On the basis of SEM images, particle size distributions were measured and are shown in Figure 2. The mean particle size (PS) and the mode of distribution are also listed in Table 1. All distributions are approximately log-normal and their mode moves from 0.26 to 0.47 μm by increasing the injector diameter. The particle size distribution (PSD) also enlarges with injector diameter, but do not vary significantly when the nozzle diameter is increased from 60 to 200 μm, that is, when the exit area is enlarged more than 1 order of magnitude. A relatively more marked variation of the mean particle diameter was observed when operating with the 500-μm nozzle. However, also in this case the mean particle diameter is small (0.57 μm). Such discrepancy could be due to the different flow arrangements between bench and pilot plant, more than to the variation of the nozzle diameter.

The weak dependence of particle diameter from the injector diameter is only apparently in contradiction with the process hydrodynamics. Indeed, classical atomization is controlled by the Weber number, that is, the ratio between inertial and surface forces, that are

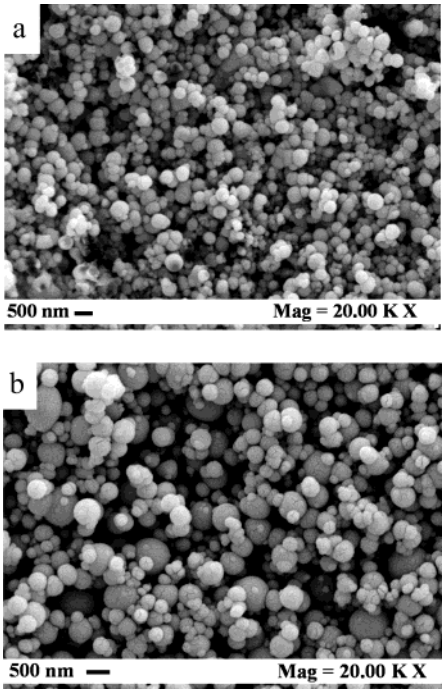

Figure 1. SEM images of YAc powders generated by SAS precipitation at 40 °C, 15 MPa, 4.5 wt % solution of YAc in DMSO: (a) 60-μm and (b) 500-μm nozzle diameter.

Table 1. Effect of the Nozzle Diameter on the Mean Particle Size (d_n) and on the Mode of the Particle Distribution of YAc Powders Obtained by SAS Precipitation from DMSO Operating at 15 MPa, 40 °C, and 4.5 wt % YAc Concentration

injector type	nozzle diameter, μm	d_n, μm	mode, μm
thin wall nozzle[a]	60	0.28	0.264
	100	0.34	0.308
	200	0.35	0.318
coaxial injector[b]	500	0.57	0.47

[a] Bench-scale apparatus. [b] Pilot-scale plant.

related to the flow velocity and to the surface tension. In the SAS process at supercritical mixture conditions, the surface tension is practically zero;[12] and thus, the Weber number-based analysis is no longer applicable. At these conditions, it is expected that a change of the liquid velocity does not affect the breakup behavior. This argument has also been proposed by Lengsfeld et al.,[12] who noted that particle size is relatively insensitive to changes in injector type and diameter. They used this experimental evidence to confute the one droplet−one particle interpretation of the SAS process.[7,23]

Effect of the Solute Concentration. The effect of the YAc concentration in the liquid solution has been studied at 40 °C, 15 MPa, and $X_{CO_2} = 0.98$. In a first set of experiments the YAc concentration has been varied between 1.36 and 13.6 wt %. These values have been chosen to operate in conditions at which the mixture DMSO/CO_2 forms a homogeneous single phase. The results have been reported in Table 2. Small particles have been obtained at all concentrations, with a slight increase of the mean particle size and distribution. SEM images taken at the same magnification are reported in Figure 3 and qualitatively show this trend in the case of 8.2 and 13.6 wt % mixtures. In a second set of experiments the pressure has been set to 12 MPa. The phase behavior study indicated that at this pressure the dilute system (1.36 wt %) forms a single phase, while the more concentrated one (4.5 wt %) crosses the transition from a monophasic to a biphasic system. The effect of the concentration on particle morphology was marked. As shown in Figure 4, nanoparticles have been obtained at 1.36 wt %; microparticles up to 10 μm in diameter have been obtained at 4.5 wt %.

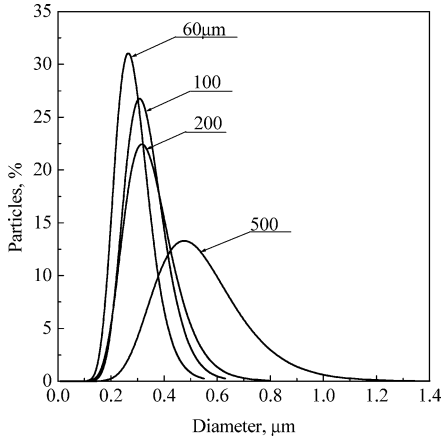

Figure 2. Effect of the injector diameter on the particle size distribution of YAc powder precipitated from DMSO at 40 °C and 15 MPa.

Effect of Pressure and Temperature. The effect of the pressure on particles morphology was studied between 7 and 15 MPa, precipitating YAc from a 1.36 wt % solution and maintaining constant all the other parameters. The results obtained for various temperatures are listed in Table 3. At 40 °C, for pressures up to 8.0 MPa a compact powder precipitated only on the bottom of the vessel. The microstructure of these materials, analyzed by SEM images, consisted of agglomerated nanoparticles whose dimension is almost constant (about 0.2 μm). As an example, in Figure 5a, a SEM image of particles obtained at 7.5 MPa is reported. As the pressure was increased to 9.0 MPa, both nano- and microparticles were present in the sample with an average particle size of 0.4 μm (Figure

Table 2. Effect of the Concentration on the Observed Particle Morphology of YAc Generated by SAS Precipitation from DMSO

temp, °C	pressure, MPa	concn, wt %	particle dimension, μm	microstructure	macrostructure
40	15	1.36[a]	0.1	nanoparticles	fine powder
	15	4.5[a]	0.28	nanoparticles	fine powder
	15	8.2[a]	0.26	nano/microparticles	fine powder
	15	13.6[a]	0.37	nano/microparticles	fine powder
50	15	4.5[b]	0.5−25	nano/microparticles	powder
60	15	4.5[b]	10−50	balloons	coarse powder
40	12	1.36[a]	0.17	nanoparticles	fine powder
	12	4.5[b]	1−15	microparticles	fine powder

[a] Laboratory-scale apparatus. [b] Pilot plant.

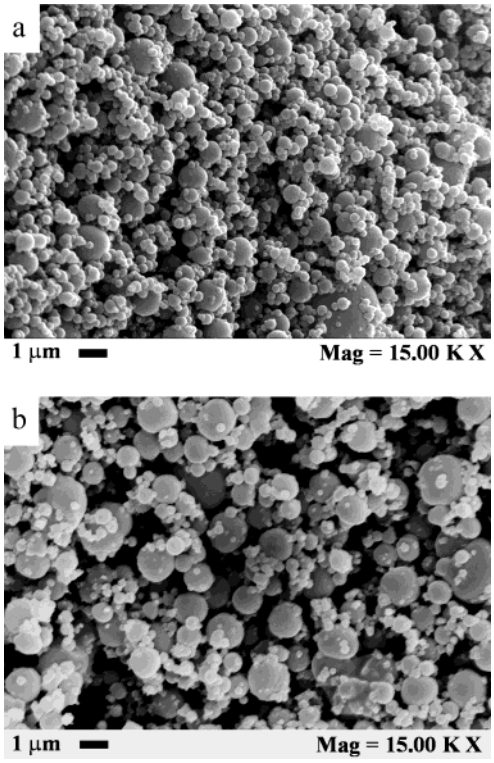

Figure 3. Effect of the YAc concentration in DMSO on the particles generated by the SAS precipitation at 40 °C, 15 MPa and (a) 8.2 and (b) 13.6 wt % concentration.

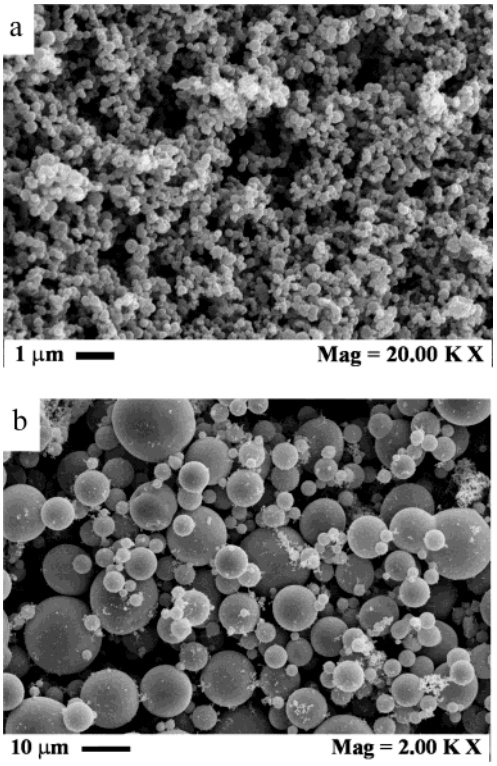

Figure 4. Effect of the YAc concentration in DMSO on the particles generated by the SAS precipitation at 40 °C and 12 MPa. (a) 1.36 and (b) 4.5 wt %.

5b). A further increase of the pressure to 9.5 MPa (i.e., the pressure at which the mixture shows a transition to monophasic behavior) causes the formation of relatively large balloon-like particles whose surface is made of many small primary particles. An example of these balloons is reported in Figure 5c. From 10 to 15 MPa, a fine powder dispersed on all of the precipitator was obtained. The microstructure of the materials is constituted by no-coalescing nanoparticles with an average diameter of about 0.1 μm (Figure 5d). The effect of the pressure on the particle morphology is reported in Table 3 also at higher temperatures. This effect is similar to that observed at 40 °C, but an increase of the pressure at which balloon-like particles are formed was observed. Indeed, at 50 °C, balloon-like particles were generated at 12 MPa, at 60 °C, balloons were generated at 14 MPa, and at 70 °C, balloons were generated at 16 MPa. In Figure 6 SEM images of these balloons obtained at 50 and 60 °C are reported. Although we are not able to give an explanation for this experimental evidence, balloon-like particles are always generated at about the same CO_2 density; i.e., from 0.56 to 0.58 g/cm^3 (see Table 3).

The effect of the temperature can also be evidenced by comparing the morphologies of particles obtained at the same pressure. For example, at 12 MPa, nanoparticles are generated at 40 °C (Figure 5d), and large balloon-like particles are generated at 50 °C (Figure 6a). This large difference of particle dimension, and the formation of balloon-like particles, also in this case is connected with a phase transition of the mixture. As shown before, at 40 °C and 12 MPa the mixture forms a stable single phase, while at 50 °C, 12 MPa is the pressure value at which the phase change occurs.

Table 3. Effect of the Pressure on the Particle Morphology of YAc Obtained by SAS Precipitation from DMSO[a]

T, °C	P, MPa	CO_2 density, g/cm^3	particles dimension, μm	microstructure	macrostructure
40	7.0	0.198	0.24	agglomerated nanoparticles	compact powder
40	7.5	0.24	0.21	agglomerated nanoparticles	compact powder
40	8.0	0.28	0.18	agglomerated nanoparticles	compact powder
40	9.0	0.484	0.4	nano/microparticles	compact powder
40	9.5	0.57	4−5	balloons	coarse powder
40	10.0	0.622	0.08	nanoparticles	fine powder
40	11.0	0.675	0.09	nanoparticles	fine powder
40	12.0	0.717	0.17	nanoparticles	fine powder
40	15.0	0.783	0.10	nanoparticles	fine powder
50	8.0	0.22	0.1	nanoparticles	compact powder
50	12.0	0.58	2−5	balloons	coarse powder
50	16.0	0.72	0.13	nanoparticles	fine powder
60	8.0	0.192	0.10	agglomerated nanoparticles	compact powder
60	14.0	0.56	3−10	balloons	coarse powder
60	16.0	0.72	0.1−2	nano + balloons	coarse powder
70	16.0	0.54	3−15	balloons	coarse powder

[a] YAc concentration = 1.36 wt %, injector diameter = 60 μm, CO_2 mass flow= 18 kg/h, DMSO mass flow= 0.67 kg/h.

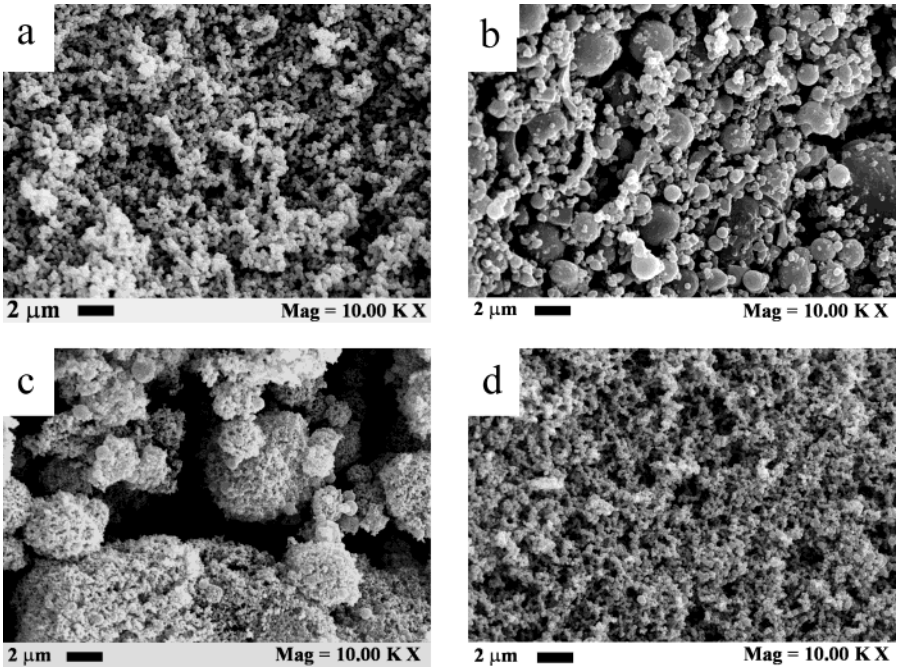

Figure 5. SEM images of YAc powders generated by SAS precipitation at 1.36 wt % of YAc in DMSO, 40 °C, and (a) 7.5, (b) 9, (c) 9.5, and (d) 12 MPa.

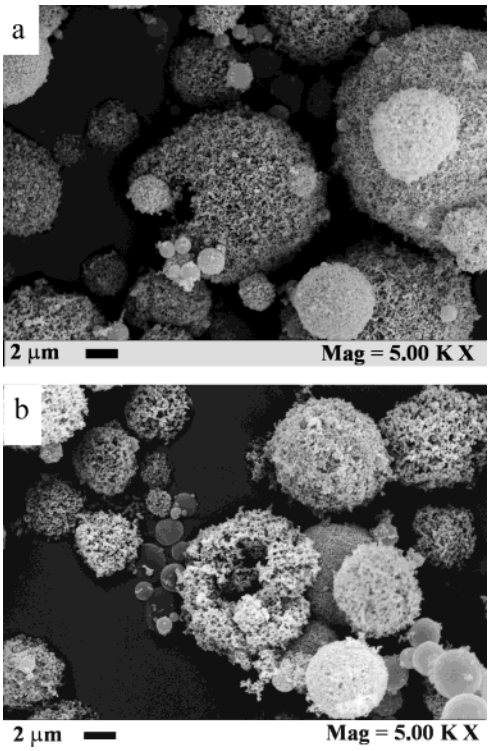

Figure 6. SEM images of balloon-like particles generated by SAS precipitation of YAc at 1.36 wt % in DMSO and (a) 50 °C/12 MPa and (b) 60 °C/14 MPa.

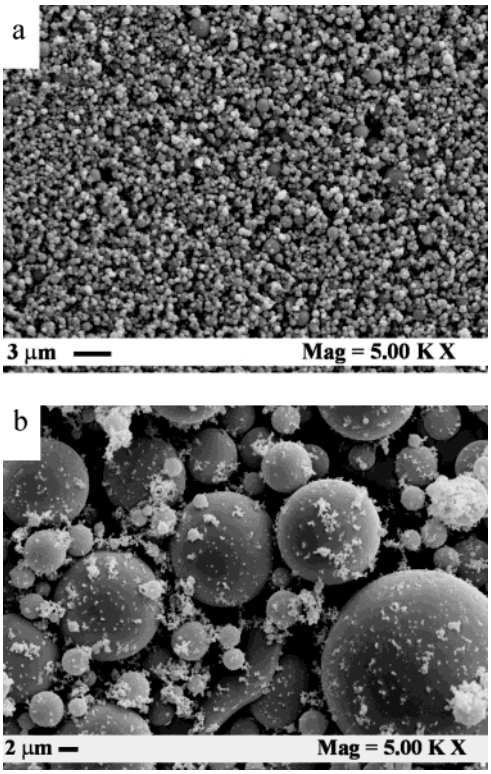

Figure 7. SEM images of YAc powders generated by SAS precipitation in the pilot plant at 4.5 wt % of YAc in DMSO, 15 MPa, and (a) 40 and (b) 50 °C.

The effect of the temperature on particle morphology was also studied at a YAc concentration of 4.5 wt %. As shown in Table 2 (rows 2, 5, and 6), in this set of experiments the temperature was increased from 40 to 60 °C, keeping constant the pressure at 15 MPa. Small spherical YAc particles (0.57-μm mean diameter) with a sharp PSD were obtained at 40 °C (Figure 7a); large particles with a continuous surface were obtained at 50 °C (Figure 7b). A further increase of the temperature up to 60 °C produces the formation of large balloon-like particles having dimension up to 50 μm. In this case some particles have the surface made of many small primary particles. Also, smaller particles having a mean dimension of about 0.2 μm are present in the sample.

Discussion

To discuss the morphologies of YAc particles obtained at different process conditions, two important considerations have to be taken into account. In the experiments carried out, for example, at 40 °C/9.5 MPa and

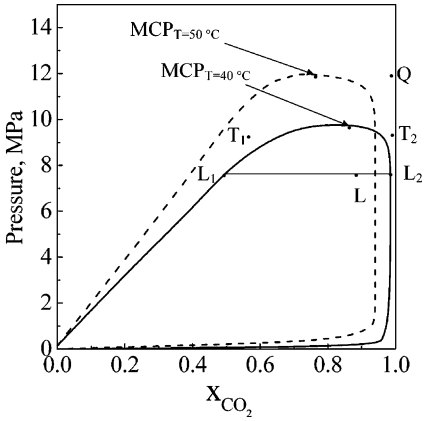

Figure 8. Tentative pseudo-binary vapor−liquid equilibrium diagram of the system DMSO/CO_2 in the presence of YAc. MCP$_{T=40°C}$ and MCP$_{T=50°C}$ are the mixture critical points; L splits into a liquid-rich (L_1) and a gas-rich (L_2) phase; T_1 is a subcritical liquid-rich phase, T_2 is a subcritical gas-rich phase; Q is the operating point for the experiments carried out at 12 MPa and $X_{CO_2} = 0.98$. Q lies in the supercritical region at 40 °C, but in the near-critical region at 50 °C. Q is the operating point for the experiments carried out at 12 MPa and $X_{CO_2} = 0.98$. Q lies in the supercritical region at 40 °C, but in the near-critical region at 50 °C.

40 °C/12 MPa (shown in Figure 5) very different particle morphologies have been generated, even if the direct observation of the phase behavior of the mixture evidenced the formation of a single phase (miscibility conditions). The second consideration concerns the role of surface tension in the particle formation mechanism. Large particles result from the formation and subsequent expansion of droplets, whose spherical shape is maintained by the surface tension between solvent and CO_2. At this point the question is: what is the relationship between morphologies and high-pressure equilibria? The vapor−liquid equilibrium of type I systems is usually reported on isothermal pressure−molar fraction diagrams ($P-x$, in the following) in which a closed loop envelops the two-phase region. A tentative $P-x$ diagram of the system DMSO/CO_2 at 40 °C is reported in Figure 8 together with some points that represent four basic phase behaviors. The diagram has been calculated using a Peng−Robinson equation of state, with interaction parameters extrapolated from the data reported by Kordikowski et al. for the system DMSO/CO_2 at 25 and 30 °C. The occurrence of the MCP at about 9.5 MPa and 40 °C is confirmed by our visual observation and by the fact that at this pressure the volumetric expansion curve of the mixture rises asymptotically.[16]

If a mixture with an overall composition L is put into the vessel, it splits into two phases: a liquid-rich phase (L_1) and a CO_2-rich phase (L_2). In both cases the CO_2 concentration is determined by the equilibrium composition. Above the mixture critical point (MCP$_{T=40°C}$ as the base case) CO_2 and the solvent are miscible in all proportions (for example, point Q in Figure 8). At Q conditions the surface tension of the liquid decreases to zero before the jet breakup and droplets do not form.[12] In the one-phase region below the MCP$_{T=40°C}$, the solvent and SC−CO_2 are still completely miscible but the mixture is subcritical. Depending on CO_2 concentration, a liquid-rich phase (T_1) or a gas-rich phase (T_2) can be formed.

This representation of the miscibility behavior could be, in a first approximation, also applied to the ternary system YAc/DMSO/CO_2. The approximation is rough, but when the solute is completely insoluble in the antisolvent (as in the case of YAc and CO_2) and is present at low concentration, it is reasonable that the system maintains the type I properties. This case is not unique; for the system DMSO/CO_2/dextrane it was shown[24] that the ternary system expansion curves overlap those of the binary system DMSO/CO_2 in the range of concentration of dextrane from 0.05 to 5 wt %. This fact means that dextrane behaves as an ideal solute that does not affect the phase behavior of the binary system solvent/antisolvent. In other cases such as, for example, the aforementioned system DMSO/CO_2/rifampicin, the solute modifies the shape of the miscibility hole and the pressure at which MCP is observed increases.[9] According to these considerations, some of the systems until now studied can be described as pseudo-binary mixtures and the $P-x$ diagram can roughly represent the ternary behavior of the mixture used in the SAS process.

Therefore, assuming that YAc at 1.36 wt % only slightly changes the phase behavior of the binary mixture CO_2/DMSO (as evidenced by the visual observation of the phase behavior), the $P-x$ diagram of Figure 8 can be used as a pseudo-binary diagram to describe the relationship between phase behavior and particle morphology. A general framework is reported here.

Case 1. If a L-type mixture is formed in the precipitator, it splits into an L1-phase, which at a high molar fraction of CO_2 occupied a very small volume, and into an L2-phase, which is the more abundant phase. The precipitation can start in the liquid-rich, in the gas-rich, or in both phases depending on the partitioning of the solute. An example of particles obtained from an L2-phase is that of YAc precipitated at 7.5 MPa and 40 °C as shown in Table 3 and Figure 5a. The phase behavior experiments confirmed the presence of an upper fluid phase from which the solute precipitated and a small liquid phase on the bottom of the precipitator. Since the precipitation occurs in a gaslike phase at a high level of supersaturation, small primary particles were formed.

The morphology of the particles obtained from an L1 mixture has been described by various authors.[8,11,25] It depends on the nucleation and growth kinetics of the material and on the degree of supersaturation of the liquid-rich phase. Examples of this behavior are represented by large crystals of grisefulvin precipitated from dicloromethane[26] and of prednisolone acetate precipitated from tetrahydrofurane.[27] In both cases the visual observation showed that two phases formed in the precipitator and crystals precipitated from a relatively small quantity of the liquid-rich phase (L_1) located at the bottom of the vessel. No precipitation was observed from the upper (L_2) fluid phase.

Another example of this behavior is represented by amoxicillin precipitated from DMSO, operating at 15 MPa, 40 °C, and 20 mg/mL. At these conditions, both crystals and amorphous particles were obtained.[27] The visual observation showed that two phases formed in the vessel and that precipitation took place from both (solute partitioning). Amorphous material precipitated from the upper phase (L2); crystals were produced from the lower phase (L1). Similar results have also been obtained in SAS precipitation of Inulin from DMSO.[28] A last example of this phase behavior is represented by ascorbic acid SAS precipitated from ethanol: crystals

at conditions below the MCP and as small particles above the MCP were obtained.[8]

Case 2. If a homogeneous supercritical phase is formed in the precipitator (Q-type mixtures, with respect to the 40 °C isotherm), particle formation results from gas-phase nucleation[12] and sub-micrometric particles are usually obtained. These experiments can be considered the most successful from the SAS micronization point of view. For example, YAc sub-micrometric particles obtained at 40 °C and 1.36 wt % (see Table 3) for pressure above 10 MPa were generated from a supercritical mixture. The very small dimension of the particles (below 0.1-μm mean diameter) (see Figure 5a) and the slight influence of the nozzle diameter indicate that droplets do not form because the surface tension decreases to zero before jet breakup. This particle formation mechanism is indicated as gas-phase nucleation.

Other examples of this behavior are dextrane sub-micrometric particles obtained from DMSO[24] samarium, neodinium, and gadolinium acetates nanoparticles produced from DMSO[16,29] and amoxicillin microparticles precipitated from *N*-methylpyrrolidone.[19]

Case 3. The precipitation from an homogeneous subcritical phase of type T_2 has not been studied before. This is the case of YAc precipitated at 40 °C/9.5 MPa. Indeed, experiments carried out with the windowed precipitator showed that CO_2 and DMSO at these conditions form an opalescent single phase very close to the transition toward the supercritical phase. At this condition when YAc was added, it precipitated in the whole volume of the chamber and balloon-like particles were obtained (see Table 3 and Figure 5c). The spherical shape of these large particles is generated by the surface tension of the liquid that is not yet zero.[5,12]

For what concerns the balloon-like particles obtained at 50 and 60 °C (Figure 6) and that obtained at 70 °C (Table 3), their morphologies can be explained considering the phase behavior of the pseudo-binary mixture CO_2/DMSO at higher temperature than 40 °C. As a rule, an increase of temperature moves the MCP of a binary mixture of type I to higher pressure.[30] This information has been indirectly verified in the case of the system CO_2/DMSO by the phase behavior study in the windowed precipitator. Indeed, it was observed that the higher the temperature, the higher the pressure at which the single phase is formed. On the basis of this qualitative information, an hypothesized miscibility diagram at 50 °C is reported in Figure 8. Therefore, nanoparticles are generated at 40 °C/12 MPa from a supercritical mixture (point Q with respect to $MCP_{T=40°C}$); balloons (see Figure 5a) are obtained at 50 °C, from a phase of type Q, that is, a subcritical single phase close to the $MCP_{T=50°C}$. When the pressure is increased above the $MCP_{T=50°C}$ (for example, at 16 MPa) a supercritical phase is formed from which nanoparticles are again generated (see Table 3). A similar approach can be followed to explain the generation of balloons obtained at 60 °C/14.0 MPa (Figure 6a) and 70 °C/16.0 MP.

The role of the solute concentration in the particle dimension and distribution can be explained starting from the results of the phase behavior study. It was shown that at higher concentration of YAc in DMSO the ternary mixture YAc/CO_2/DMSO maintains the behavior of type I systems, but an increase of the pressure at which the supercritical transition occurs is observed. Particularly at 40 °C, it increases from 9.0 to 12 MPa, increasing the concentration from 1.36 to 4.5 wt %. This experimental evidence can explain why the particles shown in Figure 4 have very different dimensions. The small one obtained at 1.36 wt % is generated from a supercritical solution following a gas-phase nucleation; the large particles obtained at 4.5 wt % are generated from a subcritical phase within discrete liquid droplets. However, the concentration of the solute can also have an effect on the nucleation kinetics of the particles precipitated from a supercritical phase. This is the case of particles precipitated at 40 °C/15 MPa, whose mean dimension slightly increases with the concentration as shown in Table 2. A similar behavior was observed also with other materials.[3,19]

Conclusions

This work confirms that SAS micronization is a highly versatile process capable of generating particles of various dimensions and morphology depending on the operating conditions. It was demonstrated that it is possible to obtain microparticles of YAc with mean diameters from 0.28 to 50 μm by simply changing the operating pressure and/or temperature and that the near-critical region can be used to impart larger dimensions and different morphologies to precipitated particles. These results have been explained on the basis of the position of the operating point with respect to the pseudo-binary MCP.

We performed experiments at the laboratory and pilot scale, showing that the scale-up of the process can be relatively simple because particle dimension and morphology are only slightly affected by jet breakup.

Our work is now addressed at confirming the experimental results by processing solutes of different chemical structure, and particularly polymers. The first results confirm that also in the case of polymers it is possible to dramatically change the particle dimension operating in the gas-rich side of the $P-x$ diagram. However, our interpretation of the role of phase behavior in the precipitation process also requires a better knowledge of the phase behavior of the ternary systems involved in the process. For this reason, the development of thermodynamic studies on the miscibility behavior of binary and ternary mixtures near the critical point should be desirable.

Literature Cited

(1) Mawson, S.; Kanakia, S.; Johnston, K. P. Coaxial nozzle for control of particle morphology in precipitation with compressed fluid antisolvent. *J. Appl. Polym. Sci.* **1997**, *64*, 2105.

(2) Jung, J.; Perrut, M. Particle design using supercritical fluids: Literature and patent survey. *J. Supercrit. Fluids* **2001**, *20*, 1.

(3) Reverchon, E. Supercritical antisolvent precipitation of micro-and nano-particles. *J. Supercrit. Fluids* **1999**, *15*, 1.

(4) Werling, J. O.; Debenedetti, P. G. Numerical modeling of mass transfer in the supercritical antisolvent process. *J. Supercrit. Fluids* **1999**, *16*, 167.

(5) Werling, J. O.; Debenedetti, P. G. Numerical modeling of mass transfer in the supercritical antisolvent process: miscible conditions. *J. Supercrit. Fluids* **2000**, *18*, 11.

(6) Kikic, I.; Bertucco, A.; Lora, M. Thermodynamic and mass transfer for the simulation of recrystallization processes with a supercritical antisolvent. In *Proceedings of the 4th Conference on Supercritical Fluids and Their Applications*; Reverchon, E., Ed.; Capri, Italy, 1997; p 299.

(7) Dixon, D. J.; Johnston, K. P.; Bodmeier, R. A. Polymeric materials formed by precipitation with a compressed fluid Antisolvent. *Mater. Interfaces Electrochem. Phenom.* **1993**, *39*, 127.

(8) Wubbolts, F. E.; Bruinsma, O. S. L.; van Rosmalen, G. M. Dry-spraying of ascorbic acid or acetaminophen solutions with supercritical carbon dioxide. *J. Cryst. Growth* **1999**, *198/199*, 767.

(9) Reverchon, E.; De Marco, I.; Della Porta, G. Rifampicin microparticles production by supercritical antisolvent precipitation. *Int. J. Pharm.* **2002**, *243* (1−2), 83.

(10) Carretier, E.; Guichardon, P.; Badens, E.; Boutin, O.; Charbit, G. Supercritical Antisolvent Process: Dissociated studies of physicochemistry and hydrodynamics. In *Proceedings of the 4th International Symposium on High-Pressure Process Technology and Chemical Engineering*; Bertucco, A., Ed.; Venice, Italy, 2002.

(11) Bristow, S.; Shekunov, T.; Shekunov, B. Yu.; York, P. Analysis of the Supersaturation and Precipitation process with supercritical CO_2. *J. Supercrit. Fluids* **2001**, *21*, 257.

(12) Lengsfeld, C. S.; Delplanque, J. P.; Barocas, V. H.; Randolph, T. W. Mechanism Governing Microparticles Morphology during Precipitation by a Compressed Antisolvent: Atomization vs Nucleation and Growth. *J. Phys. Chem. B* **2000**, *104*, 2725.

(13) Heater, K. J.; Tomansko D. L. Processing of epoxy resins using carbon dioxide as an antisolvent. *J. Supercrit. Fluids* **1998**, *14*, 55.

(14) Rantakylä, M.; Jäntti, M.; Aaltonen, O.; Hurme, M. The effect of initial droplet size on particle size in the supercritical antisolvent precipitation (SAS) technique. *J. Supercrit. Fluids* **2002**, *24*, 251.

(15) Reverchon, E.; Celano, C.; Della Porta, G. Supercritical antisolvent precipitation: A new technique for preparing submicronic yttrium powders to improve YBCO superconductor. *J. Mater. Res.* **1998**, *13* (2), 284.

(16) Reverchon, E.; Della Porta, G.; Pace, S.; Di Trolio, A. Supercritical antisolvent precipitation of submicronic particles of superconductor precursors. *Ind. Eng. Chem. Res.* **1998**, *37* (3), 952.

(17) Lavernia, E. J.; Wu, Y. *Spray atomization and deposition*; John Wiley & Son: Chichester, England, 1996.

(18) Hanna, M.; York, P. Method and Apparatus for the formation of particles. WO Patent 98/36825, 1998.

(19) Reverchon, E.; De Marco, I.; Caputo, G.; Della Porta, G. Pilot Scale Micronization of Amoxicillin by Supercritical Antisolvent Precipitation. *J. Supercrit. Fluids* **2003**, *26*, 1−7.

(20) Van Konynenburg, P. H.; Scott, R. L. Critical lines and phase equilibria in binary van der Waals mixtures. *Philos. Trans. R. Soc.* **1980**, *298*, 495.

(21) Ohe, S. *Vapor−Liquid Equilibrium Data at High Pressure*; Elsevier: Tokyo, 1990.

(22) Kordikowski, A.; Schenk, A. P.; Van Nielen, R. M.; Peters, C. J. Volume expansions and vapor-liquid equilibria of binary mixtures of a variety of polar solvents and certain near critical solvents. *J. Supercrit. Fluids* **1995**, *8*, 205.

(23) Randolph, T. W.; Randolph, A. D.; Mebes, M.; Yeung, S. Sub-micrometer-sized biodegradable particles of poly(L-lactic acid) via the gas antisolvent spray precipitation process. *Biotechnol. Prog.* **1993**, *9* (4), 429.

(24) Reverchon, E.; Della Porta, G.; De Rosa, I.; Subra, P.; Letourneur, D. Supercritical antisolvent micronization of some biopolymers. *J. Supercrit. Fluids* **2000**, *18* (3), 239.

(25) Warwick, B.; Dehghani, F.; Foster, N. R. Micronization of Copper Indomethacin Using Gas Antisolvent Processes. *Ind. Eng. Chem. Res.* **2002**, *41*, 1993.

(26) Reverchon, E.; Della Porta, G. Production of antibiotic micro- and nano-particles by supercritical antisolvent precipitation. *Powder Technol.* **1999**, *106*, 23.

(27) Reverchon, E. Micro- and Nanoparticles produced by supercritical fluid assisted techniques: present status and perspectives. In *Proceedings of the 4th International Symposium on High-Pressure Process Technology and Chemical Engineering*; Bertucco, A., Ed.; Venice, Italy, 2002.

(28) De Rosa, I. Micronizzazione di biopolimeri mediante antisolvente supercritico. Graduate Dissertation, University of Salerno, Salerno, Italy, 1998.

(29) Reverchon, E.; De Marco, I.; Della Porta, G. Tailoring of nano- and micro-particles of some superconductor precursors by supercritical antisolvent precipitation. *J. Supercrit. Fluids* **2002**, *23* (1), 81.

(30) Brunner, G. *Gas Extraction*; Springer: Berlin, 1994; pp 77, 92.

Received for review March 5, 2003
Revised manuscript received June 2, 2003
Accepted June 6, 2003

IE0302138